J Nanopart Res (2015) 17:310
DOI 10.1007/s11051-015-3114-2

REVIEW

Nanoscale luminescent lanthanide-based metal–organic frameworks: properties, synthesis, and applications

Dongqin Hu · Yonghai Song · Li Wang

Received: 1 April 2015 / Accepted: 10 July 2015 / Published online: 17 July 2015

Abstract Nanoscale luminescent lanthanide-based metal–organic frameworks (NLLn-MOFs) possess superior optical and physical properties such as higher luminescent lifetime, quantum yield, high stability, high surface area, high agent loading, and intrinsic biodegradability, and therefore are regarded as a novel generation of luminescent material compared with bulk lanthanide-based metal–organic frameworks (Ln-MOFs). Traditional luminescent Ln-MOFs have been well studied; however, NLLn-MOFs taking the advantages of nanomaterials have attracted extensive investigations for applications in optical imaging in living cells, light-harvesting, and sensing. In this review, we provide a survey of the latest progresses made in developing NLLn-MOFs, which contains the fundamental optical features, synthesis, and their potential applications. Finally, the future prospects and challenges of the rapidly growing field are summarized.

Keywords Lanthanide-based metal–organic frameworks · Luminescence · Sensing

D. Hu · Y. Song · L. Wang (✉)
Key Laboratory of Functional Small Organic Molecule, Ministry of Education, Key Laboratory of Chemical Biology, Jiangxi Province, College of Chemistry and Chemical Engineering, Jiangxi Normal University, Nanchang 330022, China
e-mail: lwanggroup@aliyun.com

Introduction

Metal–organic frameworks (MOFs) are built from metal ions (or clusters) and organic ligands through strong coordination bonds and are currently under intensive investigation as hybrid materials (An et al. 2011; Deng et al. 2010; Meek et al. 2011; Zhou et al. 2012). MOFs have emerged as interesting functional materials due to their tunable structures with high thermal stability, organic functionality, large pore sizes, high surface areas, and open metal sites in the skeleton. A wide range of applications including heterogeneous catalysis (Alaerts et al. 2006; Corma et al. 2010; Dybtsev et al. 2006; Farrusseng et al. 2009; Horike et al. 2008; Lee et al. 2009; Luz et al. 2010; Sun et al. 2009; Wu and Lin 2007; Yoon et al. 2011), gas storage and adsorption (Farha et al. 2010; Li and Yang 2007; Ma and Zhou 2010; Mulfort and Hupp 2007; Murray et al. 2009; Suh et al. 2011; Zheng et al. 2013), drug delivery and release (Horcajada et al. 2006, 2008, 2009; Taylor-Pashow et al. 2009), multimodal imaging (Rieter et al. 2006), and sensing (Achmann et al. 2009; Chen et al. 2007, 2008, 2009, 2010; Jiang et al. 2010; Kreno et al. 2011; Lu and Hupp 2010; Lu et al. 2011; Xie et al. 2009; Zhu et al. 2013) have been reported. A number of luminescent MOFs have been synthesized by taking advantage of the intrinsic fluorescence of organic bridging ligands or luminescent behaviors of the metal nodes (Chen et al. 2008; Liu et al. 2013; Wu et al. 2012). MOFs offer a platform

for the development of solid-state luminescent materials that are different from traditional inorganic complexes, because they can not only adsorb ions or molecules into the pores to allow the species to be immobilized in close proximity to luminescent centers, but also constrain the linkers inside the rigid lattice of them to increase the fluorescence lifetimes and quantum efficiencies. Therefore, luminescent MOFs are a promising class of materials that expand the applications of luminescent functional materials (Chen et al. 2007; Kuppler et al. 2009; Lee et al. 2011).

The lanthanide MOFs (Ln-MOFs) fabricated by lanthanide ions and organic linkers are a crucial member of MOFs especially luminescent MOFs. They have attracted great attention due to their good coordination characteristics and excellent optical properties, such as intense, sharp, and long lifetime, which arising from their 4*f* electrons (Zheng et al. 2012). Much attention has been paid to the design, synthesis, characterization, and application of Ln-MOFs. However, most of Ln-MOFs are bulk crystal obtained from several micrometers to millimeters, and could not always meet the practical applications. For example, most of the bulk crystals are in solid state, and this might limit the sensing in solution. Besides, the bulk sizes restrict luminescent material to interact with cells and the application in biomedicine is greatly limited (Lu et al. 2014).

With the rapid development of nanotechnology and biotechnology, especially the advances of new methods for nanomaterials synthesis, there is increasing interest in the synthesis, optical properties, and applications of nanoscale luminescent Ln-MOFs (NLLn-MOFs). Composition, structure, shape, size, spatial arrangement, and distribution of nanomaterials have great effect on the optical properties. It is certainly that NLLn-MOFs will exhibit new or superior properties due to the nanoscale effect, as compared to their bulk counterparts (Wang and Song 2006). By virtue of the size-dependent novel properties, it is desperately anticipate that versatile applications can be established. For instance, NLLn-MOFs provide sufficient small sizes to get into cells for biomedical imaging (Liu et al. 2011; Rieter et al. 2008). Besides, the high surface areas of NLLn-MOFs intensively influence and improve the photocatalysis, ion exchange, and sensing abilities. The more significant is that the small size makes it possible to design architectures with uniform sizes and well-defined materials and stable dispersion in aqueous media for improving biocompatibility or recognition capabilities (Carne et al. 2011; Horcajada et al. 2011; Keskin and Kızılel 2011; Rowe et al. 2009; Xu et al. 2011). Therefore, developing NLLn-MOFs is of great significance for biomedical and sensing applications (Horcajada et al. 2009; Liu et al. 2011; Tan and Chen 2011; Tan et al. 2012b; Taylor-Pashow et al. 2009).

However, miniaturization Ln-MOFs materials down to nanoscale is a considerable strategy to develop a new class of luminescent nanoscale materials combining the diversity of structures, properties, and compositions of classical luminescent MOFs with the obvious virtues of nanomaterials. Preparation of NLLn-MOFs is still at the early stage of development, and great efforts have been devoted to synthesize them (Lu and Yan 2014a; Vilela et al. 2014; Yi et al. 2011). As the synthesis parameters, including reactant compositions, solvents, pH, concentration, and physical conditions can influence size, crystal, and morphology of MOFs, controlling the products on the nanometers with desired properties is still a challenge. For example, You et al. demonstrated that the change of synthesis parameters such as concentration, molar ratio of reactants, surfactant, and solvent ratio led to various morphologies such as spherical, sheaf-like, wheatear-like, flower-like, taill-ike, bundle-like and nanorods with different sizes (Liu et al. 2010b).

Over the years, great attention was paid on the topic of nanomaterials and luminescent MOFs. Many significant advances have been made regarding the size and morphology control and optical performance for their applications in the fields of multimodal imaging, targeted drug deliver and treatment, light-emitting devices, and chemical sensors, as has been summarized in the recent reviews (Allendorf et al. 2009; Carne et al. 2011; Cui et al. 2011; Lin et al. 2009; Zhang et al. 2011). Although many of them have already been reviewed, it is worth underlining that this review is aimed at offering a complete review of the latest progresses of luminescent Ln-MOFs on the nanoscale regime. As shown in Fig. 1, NLLn-MOFs taking the excellent properties of luminescent Ln-MOFs and nanomaterials have demonstrated superior properties, and great efforts have devoted in their synthesis and applications. Therefore, our review focus is on their superior properties and delicate controlled synthesis of NLLn-MOFs; making use of the good dispersity, nanoscale processability, permanent porosity and high

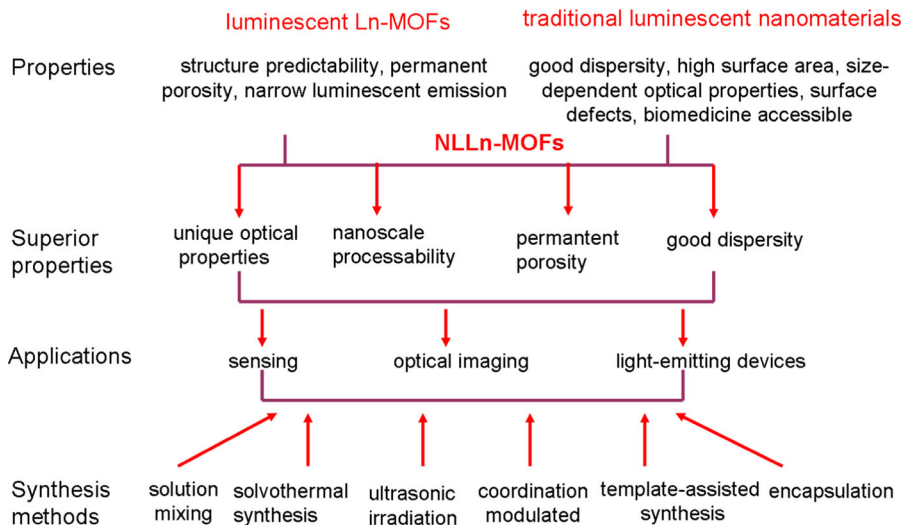

Fig. 1 Summarize of the properties, synthesis methods, and applications of NLLn-MOFs

surface area to sensitively detect guest species, and local environment; and taking advantages of the nanometer scale and biocompatibility of NLLn-MOFs to expand their usage in optical imaging. Considering the various advantages of NLLn-MOFs, they are destined to be widely investigated for practical applications in the following years.

Luminescent principle and size-dependent properties

NLLn-MOFs assembled from lanthanide ions and ligands provide a platform to generate luminescent materials upon ultraviolet excitation. As the *f–f* transitions of lanthanide ions are forbidden, it is hard to make use of the direct excitation of the lanthanide ions to generate luminescence. Ligands usually contain conjugated π moieties and it will sensitize the luminescence of lanthanide ions to induce metal-centered emission. Thus, the emission of NLLn-MOFs can be divided into three processes. (1) By coupling the lanthanide ion with organic linkers, the linkers absorb energy to immigrate from singlet state to triplet state. (2) Energy transfer from ligands to excited state of lanthanide. (3) Metal-centered emission of lanthanide ions. It is of great importance that the electronic energy level of the lowest triplet state of antenna organic linkers must be equal to or above the resonance level of the lanthanide ions to sensitize the luminescence of lanthanides. NLLn-MOFs demonstrate almost the same emission routes as that of bulk luminescent Ln-MOFs. It should be noticed that NLLn-MOFs is not to simply reduce the size of bulk luminescent Ln-MOFs, but is a kind of size-dependent nanomaterial whose luminescent properties are greatly changed. Generally speaking, NLLn-MOFs exhibit new or enhanced luminescent properties depending on the nanoscale effect and surface defects. NLLn-MOFs demonstrate stronger luminescence intensity, longer lifetime, and higher quantum yields. For instance, Zhao et al. reported that nanoscale $Tb(BTC)\cdot 6H_2O$ revealed the characteristic emission peaks at 491, 545, 590, and 624 nm, which were assigned to $^5D_4 \rightarrow {}^7F_6$, $^5D_4 \rightarrow {}^7F_5$, $^5D_4 \rightarrow {}^7F_4$, and $^5D_4 \rightarrow {}^7F_3$ transition of Tb^{3+}, respectively (Ma et al. 2010). The emission peaks were at the same position with that of bulk counterpart, but demonstrated much stronger luminescence intensity. It was ascribed to the unique size-dependent optical properties of NLLn-MOFs. Nanoscale $Tb(BTC)\cdot 6H_2O$ showed longer lifetime because of the quenching by the proximity of surface defects (Williams et al. 1998). However, the luminescence can also reveal the contrary results for the nonradiative mechanism compete with radiative mechanism. Liu et al. found that Eu-BTC bulk crystals have the strongest luminescence intensity of red light emission of Eu^{3+}, while the nanocrystals have the weakest luminescence intensity. Because the bulk crystals have fewer surface defects, and the defects in nanocrystals

form quenching centers to decrease the luminescence intensity (Xu et al. 2012a). Besides, both the bulk and nanocrystal had a long lifetime of 0.67 and 0.66 ms, respectively, which were longer than the Eu^{3+}-doped inorganic luminescent materials. Therefore, the variation of the size and structure of the crystals leads to the great changes of the optical properties of substances.

Synthesis routes for NLLn-MOFs

The precise architectural manipulation of NLLn-MOFs with well-defined morphologies and accurate tunable sizes remains a research focus. A detailed exploration of Ln-MOFs crystallization and growth processes is vital for developing a rational synthesis protocol for NLLn-MOFs (Shekhah et al. 2009). The nucleation rate of crystal growth process can be affected by reaction parameters, such as solvents, concentration of precursors, pH, temperature, and reaction time. Slight change in the parameters may lead to the varying of size and morphology. Therefore, it deserves trials to find the major influence factors that will facilitate the synthesis processes.

The synthesis routes for NLLn-MOFs are demonstrated in Fig. 2, and they can be divided into three routes. Firstly, by carefully choosing lanthanide ions and ligands to emit luminescence, we can take the advantages of the synthesis strategies of nanoscale MOFs to formulate NLLn-MOFs and it is called straightforward synthesis. Secondly, the self-assembly of merely metal ions and organic linkers sometimes cannot produce luminescent or the luminescent is very

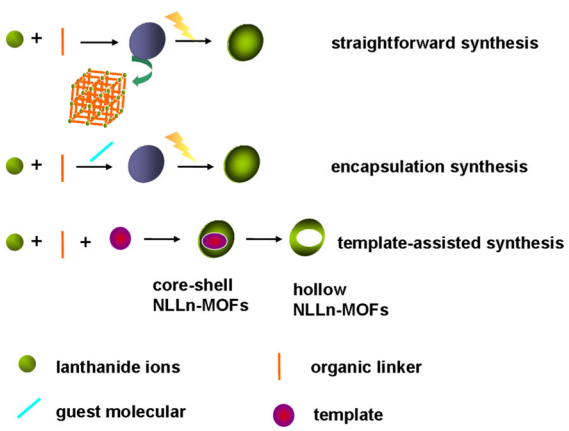

Fig. 2 Schematic of synthesis strategies of NLLn-MOFs

weak, due to the low coordination ability of organic linkers. Guest molecules such as fluorescent dyes, nanoparticles, or luminescent quantum dots (QDs) can be encapsulated into MOFs either before or after synthesizing them to generate NLLn-MOFs. Finally, nanoparticles such as gold nanoparticles and silica nanoparticles act as template to form core–shell structure or the template is removed to form hollow nanostructure, which will further improve the dispersity and surface area of nanomaterial.

Straightforward synthesis of NLLn-MOFs

Straightforward synthesis methodologies for the fabrication of NLLn-MOFs are to confine the precipitation of Ln-MOFs on the nanometer scale during the nucleation and growth process, with the help of poor solvents, thermal, ultrasounds, emulsion, microwaves, surfactants, and capping agents. As the size control of Ln-MOFs is complex, in some case, more than two conditions are employed in the synthesis process. For example, capping agents can be used in regulating the nucleation of NLLn-MOFs under heating condition (Xu et al. 2012a). Table 1 summarizes the common strategies for the straightforward synthesis of NLLn-MOFs.

Poor solvent-induced precipitation

Poor solvent-induced precipitation is a widely used approach for the synthesis of NLLn-MOFs or nanoscale luminescent coordination polymers. The strategy is that two precursors are dissolved in different solvents individually and then the precursors are mixed to induce precipitation. The other case is that the precursors are dissolved in a solvent, in which precursors and the resulted MOFs are soluble, and then a second solvent is introduced into the above system that induces the precipitation of NLLn-MOFs.

Recently, Zhang et al. fabricated NLLn-MOFs $Tb(BTC)(H_2O)_6$ with the former strategy in a facile environment and rapid way. $Tb(NO_3)_3{\cdot}6H_2O$ aqueous solution was added into H_3BTC ethanol solution under vigorous stirring at room temperature and a large amount of white precipitate occurred immediately (Yang et al. 2012). Tb^{3+} coordinated with three oxygen atoms from the carboxylate group of H_3BTC and six aqueous ligands to exhibit a one-dimensional ribbon-like structure, then a three-dimensional supramolecular

Table 1 List of straightforward synthesis method of NLLn-MOFs and their sizes and shapes

Synthesis method	NLLn-MOFs	Size	Shape	Precursor	References
Poor solvent-induced precipitation	Eu/AMP		Nanonet	$Eu(NO_3)_3{\cdot}5H_2O$, adenosine-5'-monophosphate	Tan et al. (2012b)
	$Tb(BTC)(H_2O)_6$	500 nm in length	Straw-sheaf-like	$Tb(NO_3)_3{\cdot}6H_2O$, H_3BTC	Yang et al. (2012)
	Eu-based MOF	200 nm in length and 50 nm in diameter	Block-like	$Eu(NO_3)_3{\cdot}5H_2O$, H_3BTC, sodium acetate	Choi et al. (2010)
	Tb(1,3,5-BTC)$(H_2O)\cdot 3H_2O$	Several to several hundred mm in length, 70–600 nm in width, and 10–100 nm in thickness	Nanobelt	$Ln(NO_3)_3$, H_3BTC	Liu et al. (2010a)
Solvothermal synthesis	Tb/Ad/DPA	50 nm	Spherical	$Tb(NO_3)_3$, DPA, adenine	Tan et al. (2012a)
	$Eu(BTC)(H_2O)DMF$		Urchin-like ball crystals	$Eu(NO_3)_3{\cdot}5H_2O$, H_3BTC	Liu et al. (2009)
	$Eu(BTC)(H_2O)_6$	50–100 nm in width, 10–20 nm in thickness, and several hundred nm in length	Nanorod	$Eu(NO_3)_3{\cdot}5H_2O$, H_3BTC	Xu et al. (2012a)
Ultrasonic irradiation synthesis	$Tb(BTC)(H_2O)_6$	30 in diameter and 300 nm in length	Nanowire	$Tb(NO_3)_3{\cdot}6H_2O$, H_3BTC	D'Vries et al. (2012)
Coordination-modulated synthesis	$Dy(BTC)(H_2O)$	50 nm	Spherical	$Dy(NO_3)_3$, H_3BTC, sodium acetate	Guo et al. (2012)
	$Eu_{1-x}Tb_x$-MOF	90 nm in length, 75 nm in width	Bean-shaped nanocrystals	$Eu(NO_3)_3{\cdot}5H_2O$, $Tb(NO_3)_3{\cdot}6H_2O$, H_3BTC	Cravillon et al. (2011)
	$Eu(BTC)(H_2O)DMF$	125 ± 25 nm	Belt-like and spherical	$Eu(NO_3)_3{\cdot}5H_2O$, H_3BTC, sodium acetate	Lin et al. (2009)
Microemulsion synthesis	$Eu(FMA)_2(OX)(H_2O)_4$	200–400 nm	Hexagonal	$Eu(NO_3)_3{\cdot}5H_2O$, CTAB, fumarate acid, oxalate acid	Xu et al. (2012b)
	$Eu(BDC)_{1.5}(H_2O)$	100 nm in diameter	Nanorod	$EuCl_3{\cdot}6H_2O$, H_2BDC	Rieter et al. (2006)
	$Tb(BDC)_{1.5}(H_2O)_2$	300 nm in length and 30 nm in diameter	Nanorod	$Tb(NO_3)_3{\cdot}6H_2O$, H_2BDC, $Eu(NO_3)_3{\cdot}5H_2O$, CTAB, fumarate acid, oxalate acid	Cadiau et al. (2013)
	$Eu_2(BDC)_3(H_2O)_2(H_2O)_2$	Less than 100 nm in length	Nanorod	$EuCl_3{\cdot}6H_2O$, H_2BDC	Wang et al. (2012b)

network was fabricated by π–π stacking and hydrogen bonding. SEM and X-ray diffractions were then used to characterize the crystal which exhibited a straw-sheaf-like crystals morphology with a diameter of 50 nm and a length of about 5 μm and showed a similar structure with that of simulated $Ln(BTC)(H_2O)_6$. And in the other method, the poor solvent is firstly used to mix the building blocks. The as-prepared coordination polymer

particles are with spherical morphology, which take the advantage of small surface to minimize the interfacial free energy between the particles and solvent, and exhibit an average diameter between 1 nm and several microns, relying on the specific reactions (Barrett et al. 2012; Choi et al. 2010; Cravillon et al. 2009; Lin et al. 2009; Oh and Mirkin 2006; Tan and Chen 2011; Yang et al. 2012; Zhang et al. 2011).

The latter method was reported by Choi et al. (2010), who constructed NLLn-MOFs Eu-MOF with 200 nm in length and 50 nm in diameter by slowly adding triethylamine to methanol solution containing $Eu(NO_3)_3{\cdot}5H_2O$ and H_3BTC. Poor solvent-induced fast precipitation strategy provides a relatively simple and rapid synthesis method, during which the reaction condition is easily realized to tune morphologies, sizes, and compositions of particles, and this process usually completes within hours at room temperature. However, the prepared materials are generally amorphous rather than crystalline, which prevents the detailed investigation of their inner structures.

Solvothermal method

Solvothermal method, as a typical solution-based approach, has been proven to be an effective and convenient process in preparing various materials with diverse controllable morphologies and architectures (Clausen et al. 2005; Li et al. 2008a; Wang et al. 2006). Liu et al. (2009) initially prepared well-dispersed $Eu(BTC)(H_2O)_6$ nanorods under high temperature and polar solvent. They confirmed that the formation of nanostructures was a result of the balance between the inner force and external force. The growth habit of crystal and phase structure of H_3BTC, as well as the polar solvent and high temperature contributed in the oriented nucleation, lead to the anisotropic growth of nanorods. The method is easily controllable reaction conditions, relatively large scale and high yield in terms of the quantity of desired products. It can also minimize the problem of ligand solubility, as well as enhance the reactivity of reactants, which is good for efficient molecular building during the crystallization process under forcing conditions (D'Vries et al. 2012). In addition, the method can be finely tuned so as to lead to the isolation of desired single crystals.

With the same strategy, Xu et al. (2012a) synthesized $Eu(BTC)(H_2O)DMF$ hierarchical architectures with urchin-like balls, straw-sheaf, bulk, and nanocrystals by solvothermal treatment at 60 °C for 3 days. Solvents were also reported to play a key role in the synthesis of Eu-MOFs. In the presence of co-solvent H_2O, the size can be well tuned upon variation of the DMF/H_2O molar ratio. H_2O not only acted as a reactant coordinated to metal ions, but also as a solvent to adjust the solubility of metal salts in the co-solvents in the nucleation process and crystal growth process. However, the limitation of the method is that the processes are usually time-consuming (days to weeks), bulk equipment, and heavy energy consumption.

Ultrasonic synthesis

Ultrasonic synthesis is a simple, efficient, and economic approach, which has been widely used for organic synthesis and the preparation of nanomaterials, comparing with solvothermal method (Ge and Li 2003; Kim et al. 2011; Luche and Cintas 1999). Besides, several chemical reactions that were previously hard to realize by other traditional methods can consider ultrasonic irradiation. NLLn-MOFs of nanosheets, nanorods, nanowires, and nanobelts have been synthesized (Li et al. 2008b, 2009; Qiu et al. 2008).

Hu and co-workers initially presented a facile, rapid, and environmental friendly strategy to synthesize highly one-dimensional NLLn-MOFs $Tb(BTC)(H_2O)_6$ with tunable size and shape under ultrasound irradiation at 70 °C and atmospheric pressure by varying the reaction time (Hu et al. 2012). Nanoparticles with a diameter of 50–100 nm were obtained when reacted for 5 min. However, when the time was prolonged to 30 min and even 90 min, the nanoparticles change into nanowires with a diameter of 30–50 nm along with a length of 300–500 nm (Fig. 3A) and nanorods with a diameter of 30–50 nm (Fig. 3D). All these variation are due to high transient temperatures and pressures of ultrasound irradiation condition. It accelerates the activation and the coordination reaction between lanthanide ions and H_3BTC to confine the particles in nanometer regime. Besides, the yields of nanocrystals increased from 78.2 to 83.5 %, indicating that ultrasonic method has significantly paved an efficient and rapid way to synthesize NLLn-MOFs (Li et al. 1998). Additionally, the structures of the nanocrystal were characterized by X-ray diffraction pattern, which were consisted with the simulated one, to confirm the successfully formulation of the nanorods.

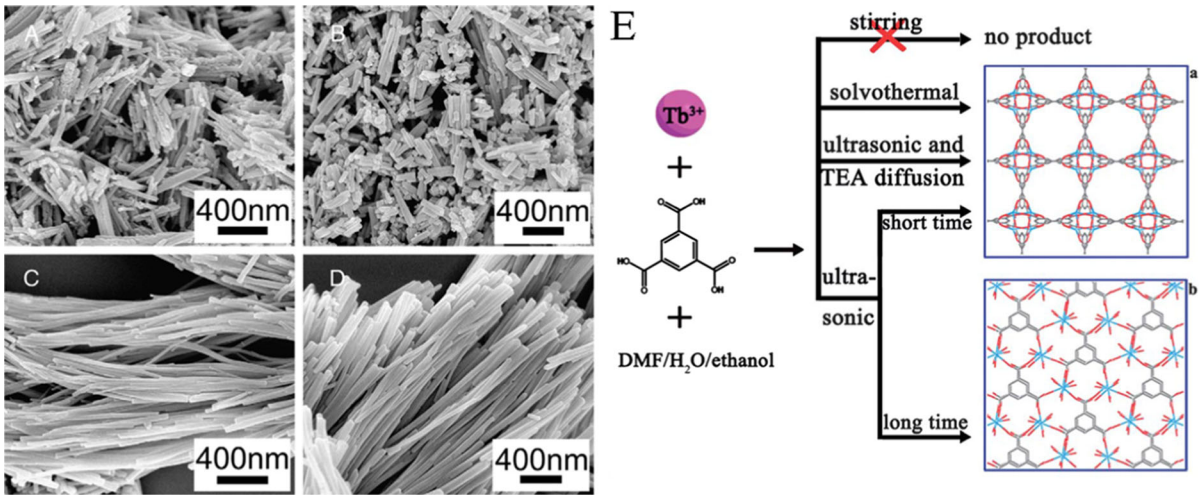

Fig. 3 SEM images of [Tb(1,3,5-BTC)$(H_2O)_6$]n synthesized using ultrasonic method for various reaction times: **A** 30, **B** 60, **C** 90, and **D** 140 min. **E** Illustration of the synthesis of terbium-based metal–organic framework crystals by various methods: **a** [Tb(1,3,5-BTC)]n 3D framework and **b** [Tb(1,3,5-BTC)$(H_2O)_6$]n 1D framework

Ultrasound-vapor phase diffusion technique is a newly technique to accelerate the reaction rate as compared with ultrasound-assisted strategy. Qiu and co-workers used an ultrasound-ethylamine (TEA) phase diffusion technique to efficiently acquire three dimension (3D) Tb(1,3,5-BTC)n nanocrystals with yields of 65.7 % in 30 min (Xiao et al. 2013). A mixture of $Tb(NO_3)_3{\cdot}6H_2O$, H_3BTC, DMF, ethanol, and H_2O was stirred for 2–4 h in a breaker and a vial filled with TEA and H_2O was placed in the breaker. Then, the reaction was conducted under ultrasonic irradiation at a frequency of 50 kHz at 60 °C and atmospheric pressure for several minutes. However, they used the ultrasound-assisted method only produced a low yield of 0.6–7.2 %. This was ascribed to the addition of deprotonation agent, TEA, which shortens the reaction time. Figure 3E describes various synthesis routes of Tb-based MOFs and found that Tb(1,3,5-BTC)n nanocrystals could change from 3D to one dimension (1D) when the ultrasonic irradiation time was long enough. Because ultrasonic could not only accelerate the chemical processes, but also may cause thermodynamic instability of the formed structure, leading to the formation of a new phase.

Coordination modulation synthesis

The coordination modulation method is a newly established and promising method for the fabrication of NLLn-MOFs. This method utilizes the strategy of modulating the coordination equilibrium by adding capping agents with the same chemical functionality as the linkers to impede the coordination interactions between metal ions and organic linkers, which generates a competitive situation that regulates the rate of framework extension and crystal growth and finally allows the control over the size and morphology of the resulting crystals. NLLn-MOFs of various shapes and sizes can be constructed by controlling the ratio of metal ions, organic linkers, solvents, and capping agents (Cravillon et al. 2011; Diring et al. 2010; Guo et al. 2010, 2012; Long et al. 2012; Nune et al. 2010; Pham et al. 2011; Tsuruoka et al. 2009; Wessels et al. 2010).

Guo et al. (2012) presented a brilliant example that illustrates how powerful can coordination modulation approach be. Combining coordination modulation with acid–base adjustment allowed the fabrication of Dy(BTC)H_2O with varying sizes and shapes. As the description of proposed Dy(BTC)H_2O crystal formation mechanism in Fig. 4A, proper acid–base environment of the reaction medium and capping agent that inhibiting crystallites from growing were two essential parameters for miniaturizing the size of Ln-MOFs crystals to nanometer scale. The efficiency of coordination modulation route to prepare NLLn-MOFs was reported by Zhang and co-workers (Guo et al. 2010). NLLn-MOFs Ln(BTC)(H_2O) was

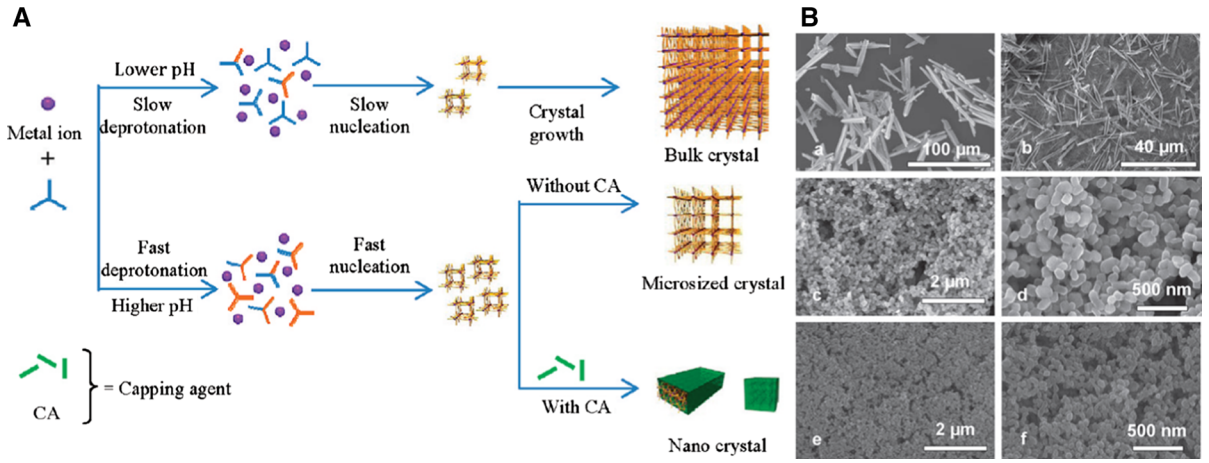

Fig. 4 **A** Proposed Dy(BTC)H_2O crystal formation mechanism. **B** SEM images of Ln-MOFs crystals synthesized: **a** without capping reagent; with addition of **b** sodium oxalate, **c**, **d** sodium formate, and **e**, **f** sodium acetate

prepared by heating a solution containing $Ln(NO_3)_3$·$5H_2O$ (0.1 mol), BTC (0.1 mol), sodium carboxylate (0–0.3 mol), DMF (8 mL), and H_2O (4 mL) in a sealed beaker at 60 °C for 12–72 h. Sodium carboxylates (sodium formate, sodium acetate, or sodium oxalate) were used as capping reagent to control the resulting crystal size and morphology. In the absence of a capping reagent, Ln-MOFs were pillar-like rods with a length of 60 ± 10 μm (Fig. 4B—a). With the addition of the capping reagent, both the shape and size of Ln-MOFs were drastically changed. Addition of sodium formate results in fairly uniform bean-shaped nanocrystals with a length and width of 125 ± 25 and 100 ± 15 nm, respectively (Fig. 4B—c, d). Smaller crystals, 90 ± 15 nm in length and 75 ± 10 nm in width were obtained, when sodium acetate was used as additive (Fig. 4B—e, f). However, sodium oxalate, led to the needle-shaped crystals (Fig. 4B—b) and the length of the crystals with lengths between 30 and 60 μm. These phenomena indicated that carboxylic salts played a crucial role in modulating the coordination interactions between lanthanide ions and organic linkers, thus provided a facile and effective way to scale down the size of Ln-MOFs.

Guo et al. described another example for the instruction of luminescent Eu-MOFs nanocrystals with different size and morphology (Xu et al. 2012a). The addition of sodium acetate from 0.1 to 0.4 mmol make the product change from belt-like and gel-like crystals to spherical monodisperse nanocrystals with a diameter of 125 ± 25 nm. And further increased of capping agent led to the aggregation of bean-like nanocrystals.

Microemulsion

Reverse or water-in-oil microemulsion technique can also adjust the dimensions of material to nanoscale, due to the well-defined volume of the underlying microreactor micelle, with sizes ranging from 50 nm to 1 μm, which was established by water to surfactant ratio (*W*) and assists in controlling the kinetics of particle nucleation and growth (Dwars et al. 2005; Rieter et al. 2006; Taylor et al. 2008).

Recently, Xu et al. (2012b) synthesized nanoscale luminescent $Eu_2(fumarate)_2(oxalate)(H_2O)_4$ by a water-in-oil microemulsion method from $Eu(NO_3)_3$, fumarate acid, oxalate acid, and different amounts of surfactants cetyltrimethylammonium bromide (CTAB) at 150 °C. Surfactants functioned as stabilizer and dispersant prevented the aggregation of nanocrystals (Ding et al. 2011; Yuan et al. 2011). As shown in Fig. 5, with the increasing amount of surfactant, the particles change from rhombus truncated bipyramidal morphology to hexagonal nanoplates. Bravais–Friedel–Donnay–Harker (BFDH) method was applied for simulating their crystal growth and morphology control, and the addition of surfactant CTAB significantly slowed down the crystal growth rate of the particles, leading to the formation of smaller micro- and nanocrystals. With the same strategy, by

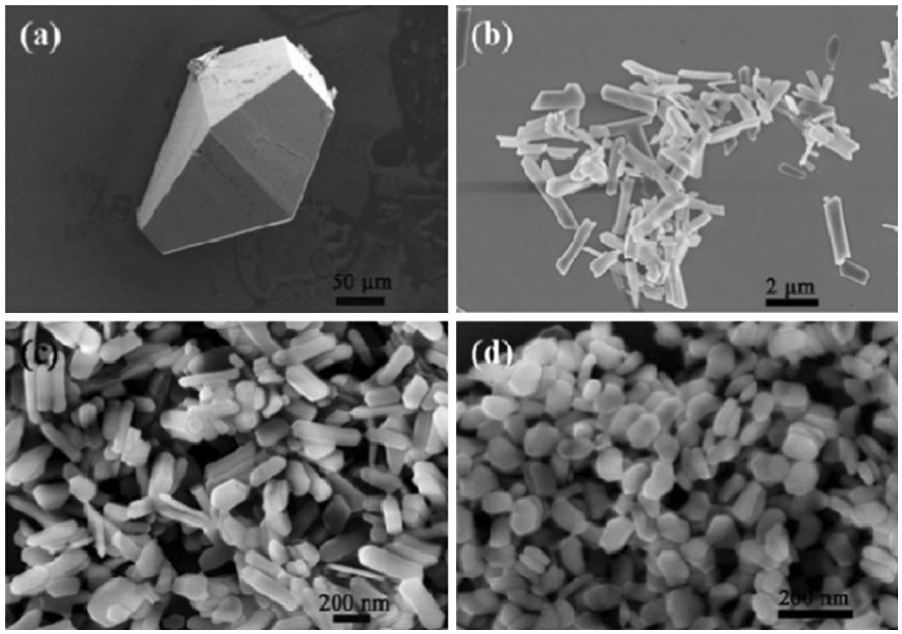

Fig. 5 SEM images of morphologies synthesized under the addition of different amounts of the CTAB modulator. **a** Large rhombus truncated bipyramid crystals synthesized without CTAB. **b** Ln-MOF elongated micrometer plates synthesized with CTAB $w = 30$. **c** Elongated hexagonal nanoplates synthesized with CTAB $w = 20$. **d** Hexagonal nanoplates synthesized with CTAB $w = 15$

dissolving $LnCl_3$ and H_2BDC in the (CTAB)/isooctane/1-hexanol/water microemulsion system, respectively, Lin et al. prepared $Ln_2(BDC)_3(H_2O)_4$ nanorods in high yield (Rieter et al. 2006). By varying W from 5 to 10, the sizes of the nanorods could be tuned from approximately 100–125 nm in length and 40 nm in diameter to 1–2 μm in length and 100 nm in diameter. Higher W values lead to larger particles because the number of nucleation sites within the microemulsion decreases. They also demonstrated that the increase of reactant concentrations leads to the formation of smaller particles, because more micelles were occupied by the reactants to generate more nucleation sites. Therefore, the use of microreactor micelle stabilized by surfactant provides a thermodynamic means to not only control the morphology during the nucleation and growth of NLLn-MOFs but also increase the stability and avoid agglomeration. The success approach to synthesize NLLn-MOFs was also confirmed by Cadiau, who fabricated $Tb(BDC)_{1.5}(H_2O)_2$ nanorod with a diameter of 30 nm and a length of 300 nm recently. Besides, Wang prepared $Eu_2(BDC)_3(H_2O)_2$ nanorod with a length less than 100 nm (Wang et al. 2012b). However, the main problem of the method is that the remove of the surfactant is time-consuming, which needs hard condition to collect the nanoscale solid. During the process, the nanoparticles may be destabilized and lead to extensive agglomeration of as-prepared primary particles.

Template-assisted synthesis of NLLn-MOFs

Template-assisted strategy takes advantage of the template core to purposely and selectively control the growth of particles, providing an excellent method to fabricate desired NLLn-MOFs or core–shell NLLn-MOFs (Hu et al. 2008; Huczko 2000; Jung et al. 2009; Shekhah et al. 2007; Perry et al. 2011; Yanagishita et al. 2005; Yang et al. 2011). Particles such as Au nanoparticles, polystyrene, and silica nanoparticles could act as templates to grow Ln-MOFs on the surface of the materials. However, the synthesis of NLLn-MOFs by template-assisted route is still rare.

Recently, Qiu et al. demonstrated template-assisted method that immobilized organic molecules onto the mercaptoacetic acid (MAA)-functionalized Fe_3O_4 NPs to construct novel Fe_3O_4@Tb-BTC core–shell structures. Fe_3O_4 NPs with a diameter of about

200 nm were added to ethanol solution of $Tb(NO_3)_3$ and H_3BTC for 30 min at 70 °C, respectively (Fig. 6a). And these processes were repeated for several cycles to obtain core–shell NLLn-MOFs (Fig. 6b). Carboxylate groups on Fe_3O_4 NPs surface interact with Ln^{3+} and initiated the growth of nanocrystals, then this interaction would induce a regular growth of Tb-BTC (Liu et al. 2012).

Encapsulation of NLLn-MOFs

Encapsulation of guest molecules into nanoscale Ln-MOFs

The highly regular channel structures and controllable pore size of nanoscale Ln-MOFs permit the encapsulation of luminescent guest molecules inside Ln-MOFs and provide another strategy to synthesize NLLn-MOFs. For example, QDs had been incorporated into Gd/AMP NCPs to formulate core–shell NLLn-MOFs (Nishiyabu et al. 2010) (Fig. 7). The shell thickness can be tunable by varying the concentration of QDs to obtain the desired sizes of particles. Luminescent QDs, metal NPs, and fluorescent dyes could be incorporated into the porous nanoscale Ln-MOFs to promote the luminescent properties of guest molecules, such as improved fluorescence intensity, efficient energy transfer, and higher quantum yields (Juan-Alcañiz et al. 2012; Tsuruoka et al. 2011; Turner et al. 2008; Wang et al. 2012a; Xiang et al. 2011). Nishiyabu et al. reported the successfully encapsulation of fluorescent guest in the coordination networks of nucleotides and lanthanide ions by electrostatic and hydrophobic interactions between molecules (Nishiyabu et al. 2009a, b, 2010). Firstly, they exploited the strategy to encapsulate three water-soluble anionic fluorescence dyes into the AMP/Lu nanoparticles (Nishiyabu et al. 2009a). Cyanine dye showed improved luminescent yields of 49 % after incorporated in the metal–organic materials comparing with 1 % of the pure dye. Besides, the luminescent intensity was greatly enhanced because the conformational rotation of the dye was restricted by Ln-MOFs to exhibit efficient energy transfer. Thus, the encapsulation of guest molecules into nanoscale Ln-MOFs might provide potential application for biomedical and material science. As for platinum porphyrin, the barrier properties of Ln-MOFs prevented the dye from oxygen quenching to exhibited high phosphorescence intensity to show light-harvesting functions. Another guest perylene dye also demonstrated strong fluorescence emission for the efficient energy transfer among ligand AMP.

Encapsulation of lanthanide ions into nanoscale MOFs

The self-assembly of merely lanthanide ions and organic linkers is sometimes nonemissive or the luminescent is very weak, due to the low coordination ability of organic linkers which allows the molecules containing high energy O–H, N–H, and C–H vibronic to compete for the coordination with lanthanide ions. Unfortunately, this prevents the further application of Ln-MOFs in optical application. However, lanthanide ions can be encapsulated into NMOFs to make lanthanide luminescence more efficiently and construct a new class of NLLn-

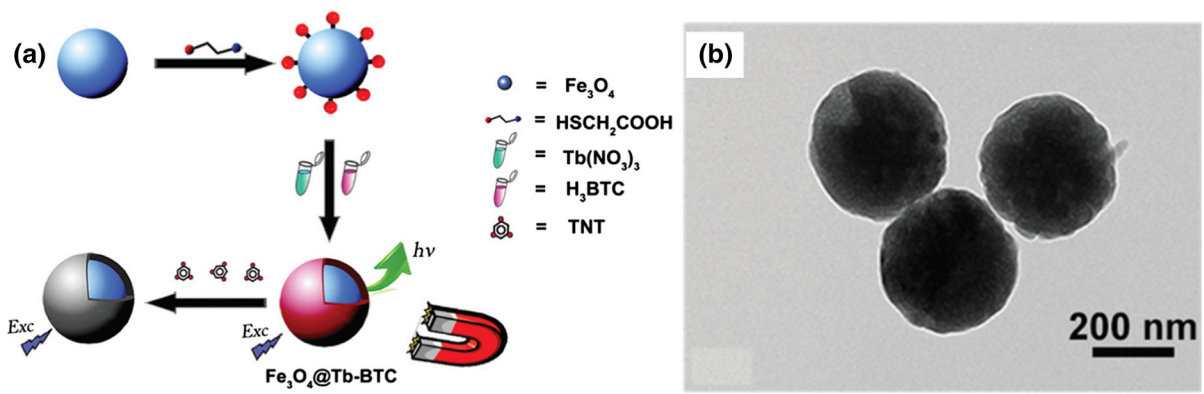

Fig. 6 **a** Schematic illustration of the fabrication process of Fe_3O_4@Tb-BTC nanospheres. **b** TEM image of Fe_3O_4@Tb-BTC nanospheres

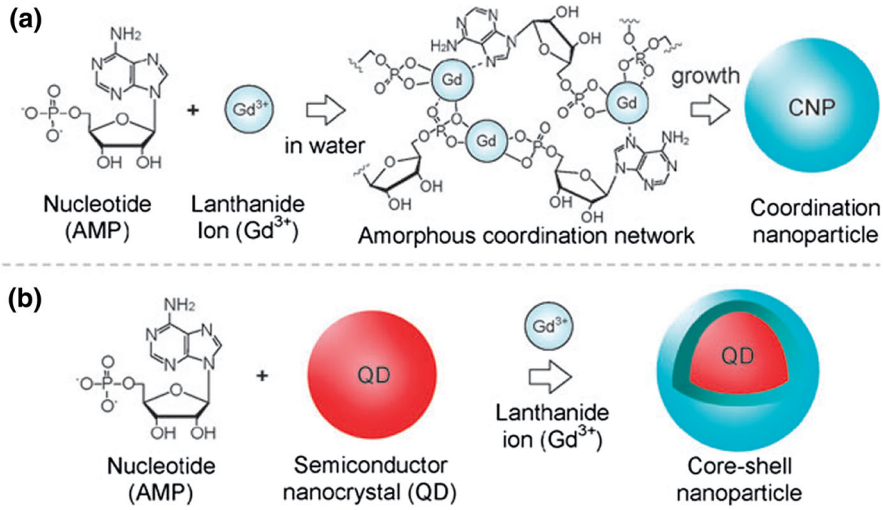

Fig. 7 **a** Formation of nanoparticles from AMP and Gd^{3+} ions. **b** Formation of QD@AMP/Gd^{3+} core–shell nanoparticles by adaptive self-assembly of AMP/Gd^{3+} networks on the surface of the QDs

MOFs. This strategy was recent demonstrated by Yan and co-workers (Zhou and Yan 2014). The highly crystalline, noncoordinating carboxyl group, as well as the high chemical and thermal stabilities of NMOFs Al-MIL-53-COOH, was good to incorporate lanthanide ions to construct Ln@Al-MIL-53-COOH. They served as a host and an antenna for sensitizing and protecting the luminescence of lanthanide ions (Fig. 8a), therefore leading to the high luminescence, high quantum yields, and long lifetime of NLLn-MOFs. In addition, emission was easily tunable by incorporating different concentrations of lanthanide ions or adjusting the excitation wavelength to induce white-light-emitting materials, which were different from the traditional lanthanide ion-doped inorganic materials, nanomaterials, and organic polymers (Fig. 8b). Another example was demonstrated by Zhou and co-workers. A MIL-type NMOFs, In(OH)(bpydc)(bpydc = 2,20-bipyridine-5,50-dicarboxylic acid), in the nanoscale range of 40–140 nm were prepared. Then NMOFs were immersed into DMF solution of chlorine salts of Eu^{3+} and Tb^{3+} to formulate Tb^{3+}/Eu^{3+}@NMOFs (Zhou et al. 2014).

Applications of NLLn-MOFs

As mentioned above, NLLn-MOFs exhibited superior properties, such as high surface areas, good dispersibility, and porosity, which paved the way for their applications in many fields, such as sensing, optical imaging, light emitting, etc. Particularly, increasing interest has focused on sensing of environmental or

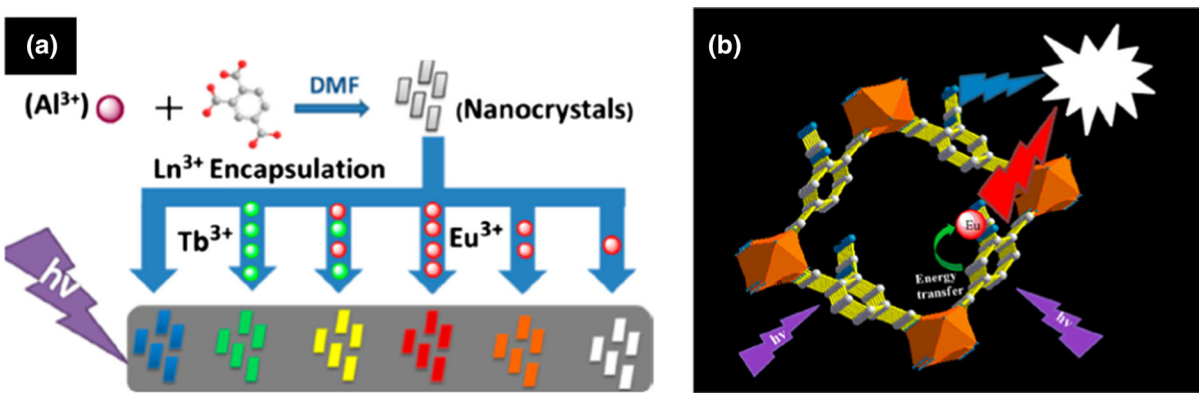

Fig. 8 **a** Encapsulation routes for Ln@Al-MIL-53-COOH. **b** Representation of the generation mechanism of the white-light emission of Eu^{3+}@Al-MIL-53-COOH

biological system in recent years, owing to the combination of permanent porosity, enhanced luminescent properties, and nanometer regime (Lu and Yan 2014b).

For example, the dispersible nature and higher surface areas of nanoscale luminescent $Eu_2(BDC)_3(H_2O)_2(H_2O)_2$ combining with the porosity of MOFs made a close contact between nanoscale MOF and solvent molecules, thus provided an excellent as well as straightforward strategy to meet the requirements of sensing for environment substances and significantly enhance the sensitivity level. While, it will be complicated to use the bulk macroscopic Ln-MOFs for sensing due to the several tedious steps including activation, incorporation of the analytes and collenction of solid Ln-MOFs. Besides, the fluorescence response rate over nanocrystals and bulk luminescent Ln-MOFs are dramatically different. It usually takes about 1 day for bulk luminescent to reach equilibrium comparing with the nanoscale luminescent Ln-MOFs only in several minutes (Tan et al. 2014). In another case, it takes about 250 s for nanocrystals to reach equilibrium, while the bulk crystals need 1500 s (Yuan et al. 2011). Nanocrystals possess a great number of porosities owing to their smaller sizes, larger surface areas as compared with their bulk crystals. The large surface areas means more reactive sites exposed to the guest molecule, as a consequence, the response rate enhanced. On the other hand, NLLn-MOFs qualify the small size for their biocompatibility to interact into cells to expand the potential applications of luminescent MOFs in optical imaging, drug delivery, etc.

Sensing

NLLn-MOFs have used as sensing platform resulting from their good luminescent properties, large surface area, good dispersibility, and porosity. The permanent porosity of porous NLLn-MOFs made it possible to selectively recognize guest species. While the special bonding sites such as open metal sites, Lewis acidic or basic sites provided different interactions with guest species will enhance the sensing sensitivity. As we have discussed above, the luminescent properties of nanoscaled Ln-MOFs were related with the coordination environment, structure of lanthanide ions, the interaction bonds with guest molecules, and the pore size. All these provided platforms to develop NLLn-MOFs for highly sensitive and selective sensing. Most of the NLLn-MOFs sensors exhibited stable, straightforward sensing property rather than the complicated sample pretreatment such as surface modification and functionalization, owing to so much activation sites of nanomaterial. Up to now, the novel materials have successfully applied in the detection of cations, such as Cu^{2+}, Ag^{+}, and Hg^{2+}, as well as molecules such as nitroaromatic explosive, aromatic amine, acetone, ciprofloxacin, dipicolinic acid (DPA), tetracycline, etc. Besides, NLLn-MOFs have been applied to detect temperature in biological recently. However, the example of NLLn-MOFs for anions detection is still rare.

Sensing of cations

The different binding interactions between free Lewis basic/acidic sites on the pore surface and metal ions incorporated into the fixed small pore of NLLn-MOFs provided a highly selective and sensitive way for the sensing of metal ions. On the other hand, the interaction between the guest species and ligands decreased the energy transfer efficiency from ligands to lanthanide ions within Ln-MOFs, leading to the decrease of fluorescent intensity.

The first example of stable porous NLLn-MOFs for Cu^{2+} sensing in aqueous solution and simulated physiological condition was reported by Xiao et al. (2010). The products exhibited a 3D framework structure with two types of micropores of about 4.0 × 5.0 Å along the *a*-axis and 3.8 × 3.8 Å along the *b*-axis, respectively, and a take-up of water vapor as high as 38 $cm^3\ g^{-1}$. The optical study found the emission spectrum of dehydrated $Eu_2(FMA)_2(OX)(H_2O)_4{\cdot}6H_2O$ (FMA = fumarate, OX = oxalate) exhibited the characteristic transitions of Eu^{3+} when excited at 394 nm. Then the effects of different cations Na^{+}, K^{+}, Mg^{2+}, Ca^{2+}, Cd^{2+}, Zn^{2+}, Pb^{2+}, Cd^{2+}, Co^{2+}, Ni^{2+}, and Cu^{2+} on the fluorescence spectrum showed that Cu^{2+} had the most significant quenching effects, thus indicated the highly selectivity of the materials. Besides, the nanostructure Ln-MOFs had a six times weaker fluorescence intensity when immersed in 0.01 M $Cu(NO_3)_2$ as compared with nonmetal-ion incorporated counterpart, accompanying with the lifetime reduced from 394.60 to 30.45 μs. Additionally, the fixed small pores within MOF enhanced the recognition of Cu^{2+} by interacting with

the terminal water or the carboxylate Lewis basic sites, leading to a remarkable highly sensitivity with a quenching coefficient of 528.7 M^{-1}, which was so much higher than that of 89.4 M^{-1} for bulk Eu-MOF for Cu^{2+} sensing. What's more, the nanostructure could be applied to sense Cu^{2+} in the simulated physiological condition due to their good dispersibility, and exhibited a comparable result with that of pure aqueous solution, which provided the potential for the forward, real time and trace amount sensing of Cu^{2+} in biological system. Another stable and dispersible nanocrystals $Tb(BTC)(H_2O)_6$ also exhibited excellent sensitive and selective sensing of Cu^{2+} (Yang et al. 2012). When the nanocrystal was dispersed in Cu^{2+} aqueous solution, the fluorescence intensity of the sample had a remark decrease at 544 nm for $^5D_4 \rightarrow {}^7F_5$ transitions of Tb^{3+}, accompanying the emitted green light significantly darker under UV light and the lifetime reduced from 0.62 to 0.37 ms.

In the other case, the fluorescence intensity of Ln-MOFs demonstrated a weak light emitting if the interaction between the ligand and lanthanide ion was too weak to be quenched by O–H oscillators of water molecules. Tan et al. reported a luminescent sensor based on metal-to-ligand charge transfer fluorescence for sensing of Ag^+ (Tan and Chen 2011). The network nanostructure Tb/AMP (AMP = adenosine monophosphate) exhibited weak luminescence, due to the weak interaction between Tb^{3+} and AMP which allowed water molecules to coordinate with Tb^{3+}. The addition of Ag^+ induced 8 times fluorescent intensity enhancement as compared with that of Tb/AMP, because the metal ions could not only interact with AMP to build a stable rigid structure to alter the excited state of AMP but also cause a more efficient intramolecular energy transfer from ligands to lanthanide ions. The fluorescence lifetime of Tb/AMP increased from 1.023 to 1.164 ms in the presence of Ag^+ further confirmed that Ag^+ was involved in the coordination site to replace the water molecules to cause a metal-to-organic charge transfer. Besides, the sensors not only exhibited fast detection time with only 7 min to reach a constant value, but also had a good linear range from 60 nM to 100 μM, along with a superior detection limit of 60 nM. The fluorescent sensor was applied in the sensing of environmental water as well, which showed a detection concentration of 80 nM and recoveries of more than 97 %. Additionally, the sensor exhibited good luminescence stability for more than 1 month, which was potential for biosensing application. The same authors demonstrated another rare luminescent nanoscale Ln-MOFs sensor based on photoinduced electron transfer (PET) for recognition and sensing of Hg^{2+} (Tan et al. 2012a). The NLLn-MOFs exhibited great selectivity and sensitivity for the sensing of Hg^{2+}, with the detection limit of 0.2 nM on the basis of a signal-to-ratio of 3:1 and a linear fluorescence response to in the concentration range of 0–100 nM (Fig. 9).

Sensing of molecules

NLLn-MOFs have found wide applications in detection of molecules. Xu et al. (2011) reported a stable and well-dispersed nanoscale luminescent $Eu_2(BDC)_3(H_2O)_2(H_2O)_2$ for straightforward and highly sensitive sensing of nitroaromatic explosives in ethanol solution. In contrast, nitroaromatic explosives including nitrobenzene, 2,4-dinitrotoluene, and 2,4,6-trinitrotoluene demonstrated an outstanding fluorescence quench effect. They discussed the possible detection mechanism was that the small pores within NLLn-MOFs stopped large aromatic from connecting with the binding sites. Besides, large surface area, good dispersibility and the pore confinement to fix the analytes within the molecular-sized cavities of nanomaterials have facilitated fast, strong, and direct interaction between analytes and nanoscale luminescent Ln-MOFs. The luminescence emission of Ln-MOFs was resulted from the antenna effects. BDC absorbed the energy and transferred to Eu^{3+} through vibronic coupling between Eu^{3+} and BDC. They explained that addition of nitroaromatic compounds caused a competition for absorption of the light source energy between the analytes and linkers. As a consequence, the energy absorption of ligands were decreased and at the same time the energy transfer from BDC to Eu^{3+} also was decreased, leading to the quenching of Eu^{3+} luminescence. Therefore, this strategy provided a promising avenue for the detection of small molecules if only we used different ligands to fabricate NLLn-MOFs to match a competition absorption with analytes.

The luminescent intensity of Ln-MOFs has also been reported to be largely dependent on the additive molecules. Usually, acetone exhibited the most significant quenching effect. The above-mentioned nanocrystal $Tb(BTC)(H_2O)_6$ showed a gradual

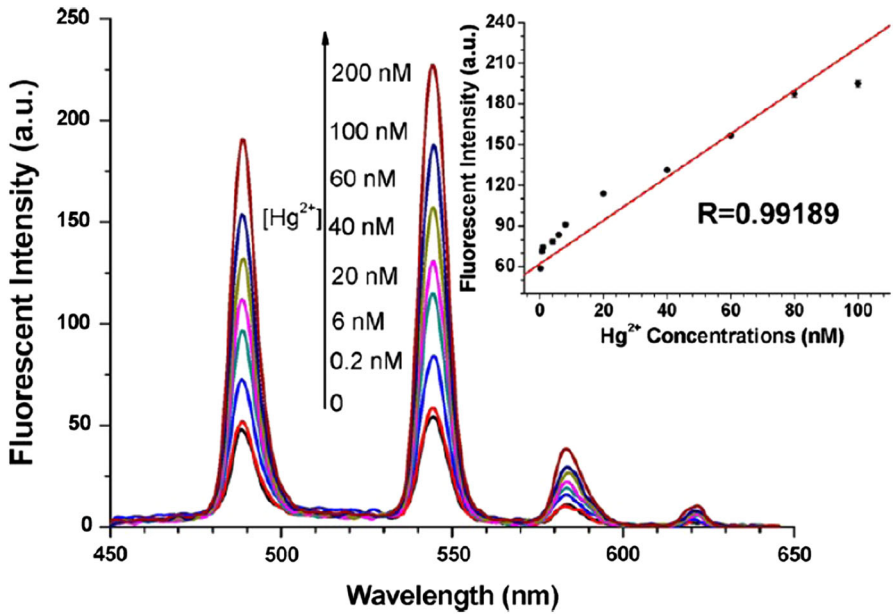

Fig. 9 Fluorescence emission spectra of Tb-MOFs in the presence of different concentrations of Hg^{2+} solution (0, 0.2, 6, 20, 40, 60, 100, 200 nM). *Inset* Linear relationship between the fluorescence intensity of nanoscale Tb-MOFs at 545 nm and Hg^{2+} concentration

luminescence decrease and red-shifted upon addition of acetone. The luminescence intensity of $^5D_4 \rightarrow {}^7F_2$ transitions of Tb^{3+} at 544 nm versus the volume ratio of acetone was well fitted by a first-order exponential decay. The suggested mechanism of quenching effects was that the physical intermolecular interaction between acetone and BTC caused energy transfer from BTC to acetone. Hu et al. (2012) reported the specific recognition functionality in $Tb(BTC)(H_2O)_6$ for aromatic amines. The sensing mechanism was that the strong supramolecular interactions such as hydrogen bonding and π–π stacking effects between the analyte molecules and ligands BTC played a crucial role in the luminescence quenching.

The nanoscale nature of NLLn-MOFs could not only easily disperse into the solvent but also significantly enhance the sensitivity level for sensing, thus exhibited great potential for trace amount detection of biomolecules. Besides, the free open luminescent lanthanide sites, such as Tb^{3+} and Eu^{3+}, played an important role in the molecular recognition, due to the binding with the substrates to cause the energy transfer from the ligands to lanthanide ions to enhance the luminescent intensity. Xu et al. (2012b) have demonstrated a luminescent $Eu_2(FMA)_2(OX)(H_2O)_4{\cdot}4H_2O$ sensor for the detection of DPA, the main component of the bacterial endospores. Adding merely 2 ppm DPA to the ethanol solution of nanomaterials obviously and instantly enhanced the fluorescence intensity and the sensitivity improved up to 90 times comparing with their bulk counterpart MOFs. They also found that the luminescent lifetime of Eu^{3+} increased with the addition of DPA, due to the binding interaction of the open Eu^{3+} sites with DPA to enforce the intramolecular energy transfer. The effects of different molecules to nanomaterial were examined, and the sensor demonstrated highly selectivity as only DPA dramatically enhanced the fluorescence intensity, while other molecules such as sodium benzoate, riboflavin, isophthalic acid, phthalic acid, and different ions were basically unchanged. This nanoscale MOFs exhibited highly sensitive, instant "turn-on" and selective sensing property, thus provided a straightforward strategy for developing new functional NLLn-MOFs for biosensing.

Recently, biology molecules such as ciprofloxacin and tetracycline have been recognized based on the open lanthanide binding sites. The nanoscale Tb/Ad not only provided high surface-to-volume ratio but also offered multiple binding sites for ciprofloxacin sensing with high detection sensitivity of 60 nM (Tan et al. 2013b). Another nanoscale Eu/AMP-Cit coordination polymer showed a fast, easy detection process as well and had a linear correlation to tetracycline from 100 nM to 20 μM (Tan et al. 2013a). It was of great significant that they had used

the nanoscale luminescent for the practical applications with good recoveries.

Sensing of temperature

Luminescent Ln-MOFs have shown versatile for the thermal detection recently. The first ratiometric luminescent Ln-MOFs thermometer sensor was demonstrated by Cui et al. (2012). The sensor demonstrated a linear correlation between luminescent and temperature in the range 50–200 K. However, cryogenic temperature and bulk particles limited the sensor for potential application in intracellular sensing. Recently, Cadiau et al. (2013) demonstrated the first stable ratiometric luminescent Ln-MOFs nanothermometer $Tb_{0.99}Eu_{0.01}(BDC)_{1.5}(H_2O)_2$, which exhibited a excellent performance in the physiological temperature range (300–320 K) with high sensitivity of 0.37 % K^{-1}. The presence of other transition of Tb^{3+} as well as the emission-decay curves of $^5D_0$ and $^5D_4$ proved energy transfer from Tb^{3+} to Eu^{3+} with energy-transfer efficiency of 23.1 %. The thermal activation of nonradiative-decay pathways resulted in the decrease of luminescent intensity of Tb^{3+} and Eu^{3+}. Therefore, the temperature dependence transitions of Tb^{3+} $^5D_4 \rightarrow {}^7F_5$ at 545 nm and Eu^{3+} $^5D_0 \rightarrow {}^7F_4$ at 698 nm provided a ratiometric thermometric parameter (Fig. 10). Another ratio of excellent luminescent thermometry Eu^{3+}/Tb^{3+}@NMOFs was reported by Zhou et al. (2014) based on the same mechanism. The ratiometric nanosensor showed a temperature range of 10–60 °C with the thermal sensitivity of 4.97 % $°C^{-1}$. Therefore, the self-referencing nanosized thermometers with high sensitivity provided the potential applications in biomedicine to measure physiological temperatures.

Optical imaging

Optical imaging is extensively used in biological studies, which uses visible light to excite dye within a tissue. However, the fluorescence of dye is easy to be photobleached at longer wavelength and the technique is limited by poor tissue penetration in vivo applications (Wessels et al. 2010). MOFs with the nanoscopic dimensions offer materials of sufficiently small sizes to get into cells to provide potential application in vitro imaging. It is noted that though several luminescent MOFs have been synthesized, most of them are limited by their low quantum yields, low fluorescence lifetime, and nonoptimal absorption properties.

NLLn-MOFs have been applied in the optical imaging; however, the examples for nanoscale luminescent Ln-MOFs were few. Lin et al. (2011) reported nanoscale Zr-MOFs with a luminescent quantum yield of 0.8 %, an average luminescence lifetime of 107 ns, and with extremely high dye loading of 57.4 %. Then Zr-MOFs were coated with silica shell to prevent rapid release from the nanoparticles and further surface modification with PEG or PEG-anisamide (AA-PEG) to be PEG-SiO_2@Zr-MOFs or AA-PEG-SiO_2@Zr-MOFs. Laser scanning confocal fluorescence microscopy studies on H460 cells were performed to investigate in vitro imaging contrast efficiency and targeting capacity. PEG-SiO_2@MOFs were proved to be efficient optical imaging contrast agents and exhibit cancer specificity, thus provided a novel platform for the design of luminescent Ln-MOFs for optical imaging.

Besides, Nishiyabu et al. (2009b) reported that fluorescent dye was incorporated during the synthesis of 5′-AMP/Gd nanoparticles to monitor their localization in cells and tissues by fluorescent microscopy in vivo. Liver toxicity result examined by enzymatic assay for aspartate aminotransferase and alanine aminotransferase indicated that the particles are nontoxic to liver, thus demonstrated the potential of dye-doped nucleotide/lanthanide nanoparticles for biological applications, especially as imaging agent for liver.

Light-emitting devices

The tunable and structural diversity of luminescent Ln-MOFs exhibited applications in white and near-infrared light emitting; however, nanoscale luminescent Ln-MOFs found applications in white and tunable light-emitting devices only in recent years. Liu et al. discussed nanobelt luminescent Tb-MOFs doped with different concentrations of Eu^{3+} ions to exhibit tunable color change from green to green-yellow, yellow, orange, and red-orange due to the energy transfer from the Tb^{3+} to Eu^{3+} ions (Liu et al. 2010a). The emission spectra gradually presented the characteristic emissions of Tb^{3+} to Eu^{3+} when the concentration increased from 0.1 to 10 mol %. Guo et al. (2010) also reported the fluorescent intensity of nanoscale $Eu_{1-x}Tb_x$-MOF changed with the ratio of lanthanide ions and demonstrated potential application in light-emitting devices.

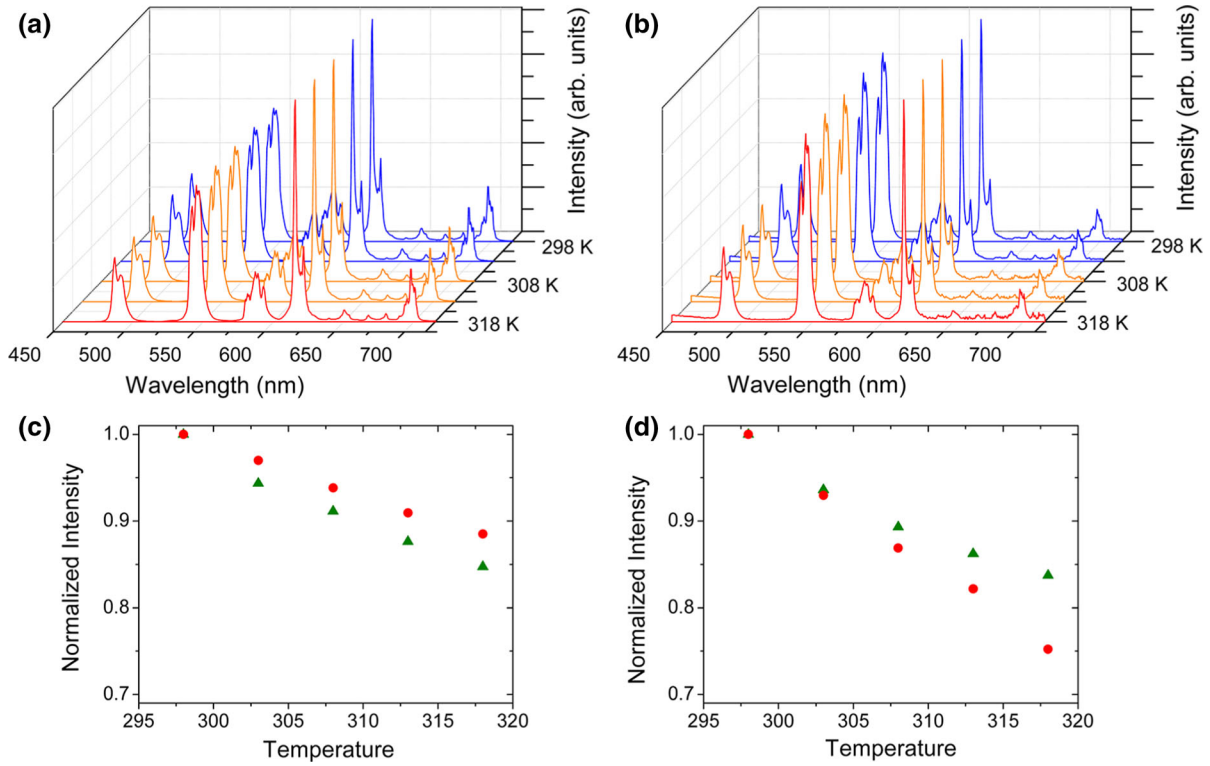

Fig. 10 Emission spectra of 1 in **a** the solid state and **b** aqueous suspension (0.36 g L^{-1}) in the physiologic temperature range excited at 320 nm. Temperature dependence of the normalized integrated intensity of the $^5D_4 \rightarrow {}^7F_5$ (Tb^{3+}, *green*) and $^5D_0 \rightarrow {}^7F_2$ (Eu^{3+}, *red*) transitions in **c** the solid state and **d** aqueous suspension. (Color figure online)

Besides, Kajsa et al. used different lanthanide ions and π-conjugated alkyl ligand (*L*) with different lengths and side chain to explore the light-harvesting properties of luminescent nanoscale Gd-MOFs (Zhang et al. 2011). The light-harvesting antenna Gd-L1-L2 was achieved by energy transfer from Gd-L1 to H_2L2 fabricated by doping the Gd-L1 with H_2L2. However, when Gd-L1 was mixed with Gd-L2 or ester, no apparent energy transfer emission was observed, which confirmed that proper organization of the donor and the acceptor could promote the energy transfer. These results have shown the excellent light-harvesting properties of nanoscale luminescent Ln-MOFs and provided strategies to enhance the optical properties of luminescent Ln-MOFs for light-emitting devices.

Conclusions and perspectives

Although the progress of NLLn-MOFs is at the infancy stage, the recent advances in this field have been illustrated and it will be convinced of a glorious future for this novel class of luminescent nanoscale materials. This review has summarized the properties, synthetic strategies, and potential applications of NLLn-MOFs. An important issue to consider is the deliberate chosen of organic linkers and metal ions to make sure the formulation of MOFs with luminescent. However, the compositions of metal ions are limited in Tb and Eu atom and organic linkers are limited in those simple linkers. It will be of challenge to apply more kinds of metal ions and linkers to build novel composite for practical applications. Another problem is to precisely control the size and morphology of luminescent Ln-MOFs on the nanometer regime for the construction of NLLn-MOFs.

From the perspective of applications, NLLn-MOFs are not only synthesized in large quantities with a desired composition, reproducible dimension, shape, and structure but also are prepared and assembled using green, environmentally responsible methodologies. So steering the size, composition, and morphology of NLLn-MOFs with exceedingly convenient and economic synthetic methodologies will be of interest.

There have been a number of achievements, including the fabrication of luminescent nanostructure with varied shapes, sizes, and compositions via different synthesis routes and controlled growth of metal–organic materials. Besides, the self-assembled properties of Ln-MOFs to encapsulate guest molecules will expand the usage of NLLn-MOFs and pave new avenue to construct multifunctional materials. Furthermore, guest molecules can be added into NLLn-MOFs, whose luminescence was quenched or very weak, and lead to the enhanced fluorescence intensity. All these are promising to improve the optical properties to develop optical devices and biological-related applications, such as light-emitting devices, optical imaging, sensing or biosensing, and so on.

However, these explorations are far beneath the demand of practical utilization, especially in biological application. The high tunable merits of NLLn-MOFs in terms of formulations, morphologies, sizes, internal structures, and properties enable the rational design for specific applications. While the main challenge is to develop more controllable synthetic methods or further understand the existing methods to sufficiently exploit the disadvantages of materials to create novel architectures with desired properties. In addition, more biological building blocks should be taken into account in the organization of luminescent nanomaterials, because the combining of biological molecules allows the biocompatibilization and easily accessing to cell-specific targets for optical imaging and biosensing of nanoscale luminescent Ln-MOFs.

Acknowledgments This work was financially supported by the National Natural Science Foundation of China (21165010, 21465014 and 21465015), Natural Science Foundation of Jiangxi Province (20142BAB203101), the Ministry of Education by the Specialized Research Fund for the Doctoral Program of Higher Education (20133604110002), the Ground Plan of Science and Technology Projects of Jiangxi Educational Committee (KJLD14023), and the Open Project Program of Key Laboratory of Functional Small Organic Molecule, Ministry of Education, Jiangxi Normal University (No. KLFS-KF-201410, KLFS-KF-201416).

References

Achmann S, Hagen G, Kita J, Malkowsky IM, Kiener C, Moos R (2009) Metal–organic frameworks for sensing applications in the gas phase. Sensors 9:1574–1589

Alaerts L, Séguin E, Poelman H, Thibault-Starzyk F, Jacobs PA, De Vos DE (2006) Probing the Lewis acidity and catalytic activity of the metal–organic framework [Cu3(btc)2](BTC = benzene-1,3,5-tricarboxylate). Chem Eur J 12:7353–7363

Allendorf M, Bauer C, Bhakta R, Houk R (2009) Luminescent metal–organic frameworks. Chem Soc Rev 38(5):1330–1352

An J, Shade CM, Chengelis-Czegan DA, Petoud S, Rosi NL (2011) Zinc-adeninate metal–organic framework for aqueous encapsulation and sensitization of near-infrared and visible emitting lanthanide cations. J Am Chem Soc 133:1220–1223

Barrett SM, Wang C, Lin W (2012) Oxygen sensing via phosphorescence quenching of doped metal–organic frameworks. J Mater Chem 22:10329–10334

Cadiau A, Brites CDS, Costa PMFJ, Ferreira RAS, Rocha J, Carlos LD (2013) Ratiometric nanothermometer based on an emissive Ln^{3+}-organic framework. ACS Nano 7:7213–7218

Carne A, Carbonell C, Imaz I, Maspoch D (2011) Nanoscale metal–organic materials. Chem Soc Rev 40:291–305

Chen B, Yang Y, Zapata F, Lin G, Qian G, Lobkovsky EB (2007) Luminescent open metal sites within a metal–organic framework for sensing small molecules. Adv Mater 19:1693–1696

Chen B, Wang L, Zapata F, Qian G, Lobkovsky EB (2008) A luminescent microporous metal–organic framework for the recognition and sensing of anions. J Am Chem Soc 130:6718–6719

Chen B, Wang L, Xiao Y, Fronczek FR, Xue M, Cui Y, Qian G (2009) A luminescent metal–organic framework with Lewis basic pyridyl sites for the sensing of metal ions. Angew Chem Int Ed 48:500–503

Chen B, Xiang S, Qian G (2010) Metal–organic frameworks with functional pores for recognition of small molecules. Acc Chem Res 43:1115–1124

Choi JR, Tachikawa T, Fujitsuka M, Majima T (2010) Europium-based metal–organic framework as a photocatalyst for the one-electron oxidation of organic compounds. Langmuir 26:10437–10443

Clausen HF, Poulsen RD, Bond AD, Chevallier M-AS, Iversen BB (2005) Solvothermal synthesis of new metal organic framework structures in the zinc–terephthalic acid–dimethyl formamide system. J Solid State Chem 178:3342–3351

Corma A, Garcia H, Llabrés i Xamena F (2010) Engineering metal organic frameworks for heterogeneous catalysis. Chem Rev 110:4606–4655

Cravillon J, Münzer S, Lohmeier S-J, Feldhoff A, Huber K, Wiebcke M (2009) Rapid room-temperature synthesis and characterization of nanocrystals of a prototypical zeolitic imidazolate framework. Chem Mater 21:1410–1412

Cravillon J, Nayuk R, Springer S, Feldhoff A, Huber K, Wiebcke M (2011) Controlling zeolitic imidazolate framework nano-and microcrystal formation: insight into crystal growth by time-resolved in situ static light scattering. Chem Mater 23:2130–2141

Cui Y, Yue Y, Qian G, Chen B (2011) Luminescent functional metal–organic frameworks. Chem Rev 112:1126–1162

Cui Y, Xu H, Yue Y, Guo Z, Yu J, Chen Z, Gao J, Yang Y, Qian G, Chen B (2012) A luminescent mixed-lanthanide metal–organic framework thermometer. J Am Chem Soc 134:3979–3982

Deng H, Doonan CJ, Furukawa H, Ferreira RB, Towne J, Knobler CB, Wang B, Yaghi OM (2010) Multiple functional groups of varying ratios in metal–organic frameworks. Science 327:846–850

Ding S-B, Wang W, Qiu L-G, Yuan Y-P, Peng F-M, Jiang X, Xie A-J, Shen Y-H, Zhu J-F (2011) Surfactant-assisted synthesis of lanthanide metal–organic framework nanorods and their fluorescence sensing of nitroaromatic explosives. Mater Lett 65:1385–1387

Diring S, Furukawa S, Takashima Y, Tsuruoka T, Kitagawa S (2010) Controlled multiscale synthesis of porous coordination polymer in nano/micro regimes. Chem Mater 22:4531–4538

D'Vries RF, Iglesias M, Snejko N, Alvarez-Garcia S, Gutiérrez-Puebla E, Monge MA (2012) Mixed lanthanide succinate–sulfate 3D MOFs: catalysts in nitroaromatic reduction reactions and emitting materials. J Mater Chem 22:1191

Dwars T, Paetzold E, Oehme G (2005) Reactions in micellar systems. Angew Chem Int Ed 44:7174–7199

Dybtsev DN, Nuzhdin AL, Chun H, Bryliakov KP, Talsi EP, Fedin VP, Kim K (2006) A homochiral metal–organic material with permanent porosity, enantioselective sorption properties, and catalytic activity. Angew Chem Int Ed 45:916–920

Farha OK, Yazaydın AÖ, Eryazici I, Malliakas CD, Hauser BG, Kanatzidis MG, Nguyen ST, Snurr RQ, Hupp JT (2010) De novo synthesis of a metal–organic framework material featuring ultrahigh surface area and gas storage capacities. Nat Chem 2:944–948

Farrusseng D, Aguado S, Pinel C (2009) Metal–organic frameworks: opportunities for catalysis. Angew Chem Int Ed 48:7502–7513

Ge J-P, Li Y-D (2003) Ultrasonic synthesis of nanocrystals of metal selenides and tellurides. J Mater Chem 13:911–915

Guo H, Zhu Y, Qiu S, Lercher JA, Zhang H (2010) Coordination Modulation induced synthesis of nanoscale $Eu_{1-x}Tb_x$-metal–organic frameworks for luminescent thin films. Adv Mater 22:4190–4192

Guo H, Zhu Y, Wang S, Su S, Zhou L, Zhang H (2012) Combining coordination modulation with acid–base adjustment for the control over size of metal–organic frameworks. Chem Mater 24:444–450

Horcajada P, Serre C, Vallet-Regí M, Sebban M, Taulelle F, Férey G (2006) Metal–organic frameworks as efficient materials for drug delivery. Angew Chem 118:6120–6124

Horcajada P, Serre C, Maurin G, Ramsahye NA, Balas F, Vallet-Regí M, Sebban M, Taulelle F, Férey G (2008) Flexible porous metal–organic frameworks for a controlled drug delivery. J Am Chem Soc 130:6774–6780

Horcajada P, Chalati T, Serre C, Gillet B, Sebrie C, Baati T, Eubank JF, Heurtaux D, Clayette P, Kreuz C (2009) Porous metal–organic-framework nanoscale carriers as a potential platform for drug delivery and imaging. Nat Mater 9:172–178

Horcajada P, Gref R, Baati T, Allan PK, Maurin G, Couvreur P, Férey G, Morris RE, Serre C (2011) Metal–organic frameworks in biomedicine. Chem Rev 112:1232–1268

Horike S, Dinca M, Tamaki K, Long JR (2008) Size-selective Lewis acid catalysis in a microporous metal–organic framework with exposed Mn^{2+} coordination sites. J Am Chem Soc 130:5854–5855

Hu JS, Zhong LS, Song WG, Wan LJ (2008) Synthesis of hierarchically structured metal oxides and their application in heavy metal ion removal. Adv Mater 20:2977–2982

Hu S-M, Niu H-L, Qiu L-G, Yuan Y-P, Jiang X, Xie A-J, Shen Y-H, Zhu J-F (2012) Facile synthesis of highly luminescent nanowires of a terbium-based metal–organic framework by an ultrasonic-assisted method and their application as a luminescent probe for selective sensing of organoamines. Inorg Chem Commun 17:147–150

Huczko A (2000) Template-based synthesis of nanomaterials. Appl Phys A 70:365–376

Jiang H-L, Tatsu Y, Lu Z-H, Xu Q (2010) Non-, micro-, and mesoporous metal–organic framework isomers: reversible transformation, fluorescence sensing, and large molecule separation. J Am Chem Soc 132:5586–5587

Juan-Alcañiz J, Gascon J, Kapteijn F (2012) Metal–organic frameworks as scaffolds for the encapsulation of active species: state of the art and future perspectives. J Mater Chem 22:10102

Jung S, Cho W, Lee HJ, Oh M (2009) Self-template-directed formation of coordination-polymer hexagonal tubes and rings, and their calcination to ZnO rings. Angew Chem Int Ed 48:1459–1462

Keskin S, Kızılel S (2011) Biomedical applications of metal organic frameworks. Ind Eng Chem Res 50:1799–1812

Kim J, Yang S-T, Choi SB, Sim J, Kim J, Ahn W-S (2011) Control of catenation in CuTATB-n metal–organic frameworks by sonochemical synthesis and its effect on CO_2 adsorption. J Mater Chem 21:3070–3076

Kreno LE, Leong K, Farha OK, Allendorf M, Van Duyne RP, Hupp JT (2011) Metal–organic framework materials as chemical sensors. Chem Rev 112:1105–1125

Kuppler RJ, Timmons DJ, Fang Q-R, Li J-R, Makal TA, Young MD, Yuan D, Zhao D, Zhuang W, Zhou H-C (2009) Potential applications of metal–organic frameworks. Coord Chem Rev 253:3042–3066

Lee J, Farha OK, Roberts J, Scheidt KA, Nguyen ST, Hupp JT (2009) Metal–organic framework materials as catalysts. Chem Soc Rev 38:1450–1459

Lee CY, Farha OK, Hong BJ, Sarjeant AA, Nguyen ST, Hupp JT (2011) Light-harvesting metal–organic frameworks (MOFs): efficient strut-to-strut energy transfer in bodipy and porphyrin-based MOFs. J Am Chem Soc 133: 15858–15861

Li Y, Yang RT (2007) Gas adsorption and storage in metal–organic framework MOF-177. Langmuir 23:12937–12944

Li H, Eddaoudi M, Groy TL, Yaghi O (1998) Establishing microporosity in open metal–organic frameworks: gas sorption isotherms for Zn (BDC)(BDC = 1,4-benzenedicarboxylate). J Am Chem Soc 120:8571–8572

Li C, Yang J, Yang P, Lian H, Lin J (2008a) Hydrothermal synthesis of lanthanide fluorides LnF_3 (Ln = La to Lu) nano-/microcrystals with multiform structures and morphologies. Chem Mater 20:4317–4326

Li Z-Q, Qiu L-G, Wang W, Xu T, Wu Y, Jiang X (2008b) Fabrication of nanosheets of a fluorescent metal–organic framework [Zn (BDC)(H_2O)]n (BDC = 1,4-benzenedicarboxylate): ultrasonic synthesis and sensing of ethylamine. Inorg Chem Commun 11:1375–1377

Li Z-Q, Qiu L-G, Xu T, Wu Y, Wang W, Wu Z-Y, Jiang X (2009) Ultrasonic synthesis of the microporous metal–

organic framework $Cu_3(BTC)_2$ at ambient temperature and pressure: an efficient and environmentally friendly method. Mater Lett 63:78–80

Lin W, Rieter WJ, Taylor KM (2009) Modular synthesis of functional nanoscale coordination polymers. Angew Chem Int Ed 48(4):650–658

Liu K, You H, Jia G, Zheng Y, Song Y, Yang M, Huang Y, Zhang H (2009) Coordination-induced formation of one-dimensional nanostructures of europium benzene-1,3,5-tricarboxylate and its solid-state thermal transformation. Cryst Growth Des 9:3519–3524

Liu K, You H, Zheng Y, Jia G, Song Y, Huang Y, Yang M, Jia J, Guo N, Zhang H (2010a) Facile and rapid fabrication of metal–organic framework nanobelts and color-tunable photoluminescence properties. J Mater Chem 20:3272–3279

Liu K, Zheng Y, Jia G, Yang M, Song Y, Guo N, You H (2010b) Nano/micro-scaled La(1,3,5-BTC)(H_2O)6 coordination polymer: facile morphology-controlled fabrication and color-tunable photoluminescence properties by co-doping Eu^{3+}, Tb^{3+}. J Solid State Chem 183:2309–2316

Liu D, Huxford RC, Lin W (2011) Phosphorescent nanoscale coordination polymers as contrast agents for optical imaging. Angew Chem Int Ed Engl 123:3780–3784

Liu J-M, L-p Lin, Wang X-X, Lin S-Q, Cai W-L, Zhang L-H, Zheng Z-Y (2012) Highly selective and sensitive detection of Cu^{2+} with lysine enhancing bovine serum albumin modified-carbon dots fluorescent probe. Analyst 137: 2637–2642

Liu G-l, Qin Y-j, Jing L, Wei G-y, Li H (2013) Two novel MOF-74 analogs exhibiting unique luminescent selectivity. Chem Commun (Camb) 49:1699–1701

Long J, Wang S, Ding Z, Wang S, Zhou Y, Huang L, Wang X (2012) Amine-functionalized zirconium metal–organic framework as efficient visible-light photocatalyst for aerobic organic transformations. Nat Chem 48:11656–11658

Lu G, Hupp JT (2010) Metal–organic frameworks as sensors: a ZIF-8 based Fabry–Pérot device as a selective sensor for chemical vapors and gases. J Am Chem Soc 132:7832–7833

Lu Y, Yan B (2014a) Luminescent lanthanide barcodes based on postsynthetic modified nanoscale metal–organic frameworks. J Mater Chem C 2:7411–7416

Lu Y, Yan B (2014b) A ratiometric fluorescent pH sensor based on nanoscale metal–organic frameworks (MOFs) modified by europium(III complexes. Chem Commun 50:13323–13326

Lu W, Qin X, Luo Y, Chang G, Sun X (2011) CdS quantum dots as a fluorescent sensing platform for nucleic acid detection. Microchim Acta 175:355–359

Lu Y, Yan B, Liu J-L (2014) Nanoscale metal–organic frameworks as highly sensitive luminescent sensors for Fe^{2+} in aqueous solution and living cells. Chem Commun 50: 9969–9972

Luche J-L, Cintas P (1999) Can sonication modify the regio and stereoselectivities of organic reactions? Adv Sonochem 5:147–174

Luz I, Llabrés i Xamena F, Corma A (2010) Bridging homogeneous and heterogeneous catalysis with MOFs: "Click" reactions with Cu-MOF catalysts. J Catal 276:134–140

Ma S, Zhou H-C (2010) Gas storage in porous metal–organic frameworks for clean energy applications. Chem Commun 46:44–53

Ma R, Chu H, Zhao Y, Wuren Q, Shan M (2010) Synthesis and fluorescence properties of ten lanthanide benzene-1,3,5-tricarboxylate complexes. Spectrochim Acta A 77:419–423

Meek ST, Greathouse JA, Allendorf MD (2011) Metal–organic frameworks: a rapidly growing class of versatile nanoporous materials. Adv Mater 23:249–267

Mulfort KL, Hupp JT (2007) Chemical reduction of metal–organic framework materials as a method to enhance gas uptake and binding. J Am Chem Soc 129:9604–9605

Murray LJ, Dincă M, Long JR (2009) Hydrogen storage in metal–organic frameworks. Chem Soc Rev 38:1294–1314

Nishiyabu R, Aime C, Gondo R, Noguchi T, Kimizuka N (2009a) Confining molecules within aqueous coordination nanoparticles by adaptive molecular self-assembly. Angew Chem Int Ed Engl 48:9465–9468

Nishiyabu R, Hashimoto N, Cho T, Watanabe K, Yasunaga T, Endo A, Kaneko K, Niidome T, Murata M, Adachi C (2009b) Nanoparticles of adaptive supramolecular networks self-assembled from nucleotides and lanthanide ions. J Am Chem Soc 131:2151–2158

Nishiyabu R, Aime C, Gondo R, Kaneko K, Kimizuka N (2010) Selective inclusion of anionic quantum dots in coordination network shells of nucleotides and lanthanide ions. Chem Commun (Camb) 46:4333–4335

Nune SK, Thallapally PK, Dohnalkova A, Wang C, Liu J, Exarhos GJ (2010) Synthesis and properties of nano zeolitic imidazolate frameworks. Chem Commun 46:4878–4880

Oh M, Mirkin CA (2006) Ion exchange as a way of controlling the chemical compositions of nano- and microparticles made from infinite coordination polymers. Angew Chem Int Ed Engl 118:5618–5620

Perry JL, Martin CR, Stewart JD (2011) Drug-delivery strategies by using template-synthesized nanotubes. Chem Eur J 17:6296–6302

Pham M-H, Vuong G-T, Vu A-T, Do T-O (2011) Novel route to size-controlled Fe-MIL-88B-NH2 metal–organic framework nanocrystals. Langmuir 27(24):15261–15267

Qiu L-G, Li Z-Q, Wu Y, Wang W, Xu T, Jiang X (2008) Facile synthesis of nanocrystals of a microporous metal–organic framework by an ultrasonic method and selective sensing of organoamines. Chem Commun 31:3642–3644

Rieter WJ, Taylor KML, An HY, Lin WL, Lin WB (2006) Nanoscale metal–organic frameworks as potential multimodal contrast enhancing agents. J Am Chem Soc 128: 9024–9025

Rieter WJ, Pott KM, Taylor KM, Lin W (2008) Nanoscale coordination polymers for platinum-based anticancer drug delivery. J Am Chem Soc 130:11584–11585

Rowe MD, Thamm DH, Kraft SL, Boyes SG (2009) Polymer-modified gadolinium metal–organic framework nanoparticles used as multifunctional nanomedicines for the targeted imaging and treatment of cancer. Biomacromolecules 10: 983–993

Shekhah O, Wang H, Kowarik S, Schreiber F, Paulus M, Tolan M, Sternemann Ch, Evers F, Zacher D, Fischer RA, Wöll Ch (2007) Step-by-step route for the synthesis of metal–organic frameworks. J Am Chem Soc 129:15118–15119

Shekhah O, Wang H, Zacher D, Fischer RA, Wöll C (2009) Growth mechanism of metal–organic frameworks: insights into the nucleation by employing a step-by-step route. Angew Chem Int Ed 48:5038–5041

Suh MP, Park HJ, Prasad TK, Lim D-W (2011) Hydrogen storage in metal–organic frameworks. Chem Rev 112:782–835

Sun C-Y, Liu S-X, Liang D-D, Shao K-Z, Ren Y-H, Su Z-M (2009) Highly stable crystalline catalysts based on a microporous metal–organic framework and polyoxometalates. J Am Chem Soc 131:1883–1888

Tan H, Chen Y (2011) Ag(+)-enhanced fluorescence of lanthanide/nucleotide coordination polymers and Ag(+) sensing. Chem Commun (Camb) 47:12373–12375

Tan H, Liu B, Chen Y (2012a) Lanthanide coordination polymer nanoparticles for sensing of Mercury (II) by photoinduced electron transfer. ACS Nano 6:10505–10511

Tan H, Liu B, Chen Y (2012b) Luminescence nucleotide/Eu^{3+} coordination polymer based on the inclusion of tetracycline. J Phys Chem C 116:2292–2296

Tan H, Ma C, Song Y, Xu F, Chen S, Wang L (2013a) Determination of tetracycline in milk by using nucleotide/lanthanide coordination polymer-based ternary complex. Biosens Bioelectron 50:447–452

Tan H, Zhang L, Ma C, Song Y, Xu F, Chen S, Wang L (2013b) Terbium-based coordination polymer nanoparticles for detection of ciprofloxacin in tablets and biological fluids. ACS Appl Mater Interfaces 5:11791–11796

Tan H, Ma C, Chen L, Xu F, Chen S, Wang L (2014) Nanoscaled lanthanide/nucleotide coordination polymer for detection of an anthrax biomarker. Sens Actuators B 190:621–626

Taylor KM, Rieter WJ, Lin W (2008) Manganese-based nanoscale metal–organic frameworks for magnetic resonance imaging. J Am Chem Soc 130:14358–14359

Taylor-Pashow KM, Rocca JD, Xie Z, Tran S, Lin W (2009) Postsynthetic modifications of iron-carboxylate nanoscale metal–organic frameworks for imaging and drug delivery. J Am Chem Soc 131:14261–14263

Tsuruoka T, Furukawa S, Takashima Y, Yoshida K, Isoda S, Kitagawa S (2009) Nanoporous nanorods fabricated by coordination modulation and oriented attachment growth. Angew Chem Int Ed 48:4739–4743

Tsuruoka T, Kawasaki H, Nawafune H, Akamatsu K (2011) Controlled self-assembly of metal–organic frameworks on metal nanoparticles for efficient synthesis of hybrid nanostructures. ACS Appl Mater Interfaces 3(10):3788–3791

Turner S, Lebedev OI, Schröder F, Esken D, Fischer RA, Tendeloo GV (2008) Direct imaging of loaded metal–organic framework materials (metal@MOF-5). Chem Mater 20:5622–5627

Vilela SM, Ananias D, Fernandes JA, Silva P, Gomes AC, Silva NJ, Rodrigues MO, Tomé JP, Valente AA, Ribeiro-Claro P (2014) Multifunctional micro- and nanosized metal–organic frameworks assembled from bisphosphonates and lanthanides. J Mater Chem C 2:3311–3327

Wang ZL, Song J (2006) Piezoelectric nanogenerators based on zinc oxide nanowire arrays. Science 312:242–246

Wang X, Zhuang J, Peng Q, Li Y (2006) Hydrothermal synthesis of rare-earth fluoride nanocrystals. Inorg Chem 45:6661–6665

Wang C, deKrafft KE, Lin W (2012a) Pt nanoparticles@photoactive metal–organic frameworks: efficient hydrogen evolution via synergistic photoexcitation and electron injection. J Am Chem Soc 134:7211–7214

Wang Y-P, Wang F, Luo D-F, Zhou L, Wen L-L (2012b) A luminescent nanocrystal metal–organic framework for sensing of nitroaromatic compounds. Inorg Chem Commun 19:43–46

Wessels JT, Yamauchi K, Hoffman RM, Wouters FS (2010) Advances in cellular, subcellular, and nanoscale imaging in vitro and in vivo. Cytometry 77:667–676

Williams DK, Bihari B, Tissue BM, McHale JM (1998) Preparation and fluorescence spectroscopy of bulk monoclinic Eu^{3+}: Y_2O_3 and comparison to Eu^{3+}: Y_2O_3 nanocrystals. J Phys Chem B 102:916–920

Wu CD, Lin W (2007) Heterogeneous asymmetric catalysis with homochiral metal–organic frameworks: network-structure-dependent catalytic activity. Angew Chem Int Ed 119:1093–1096

Wu P, Wang J, He C, Zhang X, Wang Y, Liu T, Duan C (2012) Luminescent metal–organic frameworks for selectively sensing nitric oxide in an aqueous solution and in living cells. Adv Funct Mater 22:1698–1703

Xiang Z, Hu Z, Cao D, Yang W, Lu J, Han B, Wang W (2011) Metal–organic frameworks with incorporated carbon nanotubes: improving carbon dioxide and methane storage capacities by lithium doping. Angew Chem Int Ed 50:491–494

Xiao Y, Cui Y, Zheng Q, Xiang S, Qian G, Chen B (2010) A microporous luminescent metal–organic framework for highly selective and sensitive sensing of Cu^{2+} in aqueous solution. Chem Commun 46(30):5503–5505

Xiao J-D, Qiu L-G, Ke F, Yuan Y-P, Xu G-S, Wang Y-M, Jiang X (2013) Rapid synthesis of nanoscale terbium-based metal–organic frameworks by a combined ultrasound-vapour phase diffusion method for highly selective sensing of picric acid. J Mater Chem A 1:8745–8752

Xie Z, Ma L, deKrafft KE, Jin A, Lin W (2009) Porous phosphorescent coordination polymers for oxygen sensing. J Am Chem Soc 132:922–923

Xu H, Liu F, Cui Y, Chen B, Qian G (2011) A luminescent nanoscale metal–organic framework for sensing of nitroaromatic explosives. Chem Commun (Camb) 47(11): 3153–3155

Xu B, Guo H, Wang S, Li Y, Zhang H, Liu C (2012a) Solvothermal synthesis of luminescent Eu(BTC)(H_2O)DMF hierarchical architectures. CrystEngComm 14: 2914–2919

Xu H, Rao X, Gao J, Yu J, Wang Z, Dou Z, Cui Y, Yang Y, Chen B, Qian G (2012b) A luminescent nanoscale metal–organic framework with controllable morphologies for spore detection. Chem Commun 48:7377–7379

Yanagishita T, Nishio K, Masuda H (2005) Fabrication of metal nanohole arrays with high aspect ratios using two-step replication of anodic porous alumina. Adv Mater 17: 2241–2243

Yang X, Tang H, Cao K, Song H, Sheng W, Wu Q (2011) Templated-assisted one-dimensional silica nanotubes: synthesis and applications. J Mater Chem 21:6122–6135

Yang W, Feng J, Zhang H (2012) Facile and rapid fabrication of nanostructured lanthanide coordination polymers as selective luminescent probes in aqueous solution. J Mater Chem 22:6819

Yi X-Y, Fang H-C, Gu Z-G, Zhou Z-Y, Cai Y-P, Tian J, Thallapally PK (2011) Metal–organic frameworks with achiral/monochiral nano-channels. Cryst Growth Des 11: 2824–2828

Yoon M, Srirambalaji R, Kim K (2011) Homochiral metal–organic frameworks for asymmetric heterogeneous catalysis. Chem Rev 112:1196–1231

Yuan Y, Wang W, Qiu L, Peng F, Jiang X, Xie A, Shen Y, Tian X, Zhang L (2011) Surfactant-assisted facile synthesis of fluorescent zinc benzenedicarboxylate metal–organic framework nanorods with enhanced nitrobenzene explosives detection. Mater Chem Phys 131:358–361

Zhang X, Ballem MA, Hu ZJ, Bergman P, Uvdal K (2011) Nanoscale light-harvesting metal–organic frameworks. Angew Chem Int Ed Engl 123:5847–5851

Zheng B, Zhang D, Peng Y, Huo Q, Liu Y (2012) Syntheses, structures and luminescence properties of two novel lanthanide metal–organic frameworks based on a rigid tetracarboxylate ligand. Inorg Chem Commun 16:70–73

Zheng B, Yun R, Bai J, Lu Z, Du L, Li Y (2013) Expanded Porous MOF-505 analogue exhibiting large hydrogen storage capacity and selective carbon dioxide adsorption. Inorg Chem 52:2823–2829

Zhou Y, Yan B (2014) Imparting Tunable and white-light luminescence to a nanosized metal–organic framework by controlled encapsulation of lanthanide cations. Inorg Chem 53:3456–3463

Zhou H-C, Long JR, Yaghi OM (2012) Introduction to metal–organic frameworks. Chem Rev 112(2):673–674

Zhou Y, Yan B, Lei F (2014) Postsynthetic lanthanide functionalization of nanosized metal–organic frameworks for highly sensitive ratiometric luminescent thermometry. Chem Commun 50:15235–15238

Zhu X, Zheng H, Wei X, Lin Z, Guo L, Qiu B, Chen G (2013) Metal–organic framework (MOF): a novel sensing platform for biomolecules. Chem Commun 49:1276–1278